© The Author(s) 2018

Kaiheng Hu · Chaohua Wu · Jinbo Tang · Alessandro Pasuto · Yanji Li · Shuaixing Yan

New understandings of the June 24th 2017 Xinmo Landslide, Maoxian, Sichuan, China

Abstract On June 24, 2017 (21:39 UTC, June 23rd), a catastrophic landslide occurred at Xinmo village of Mao County, Sichuan Province, China. Soon after the event, some research teams carried out field investigations in order to both support the emergency operations and to understand the failure mechanism and possible evolutionary scenarios. Based on further in-depth interpretation of high-resolution remote-sensing images and detailed field surveys, it is newly found that there are at least six old rockfall deposits in the source area that prove the historic activity of the landslide scarp. Seismic data of the event and morphological evidences along the slope indicate that the landslide was preceded by a significant rockfall. Mechanical calculations show that the surface force due to pore water was far less than the impact force due to the rockfall. It means that the subsequent major rock avalanche was more likely due to the impact of the rockfall on the rock slope below, which broke the rock bridges and caused drop of shear resistance along the fractures. According to these new understandings, a different triggering mechanism for the landslide is proposed.

Keywords Xinmo landslide · Triggering mechanism · Rockfall-debris avalanche

Introduction

Large-volume landslides represent a persistent threat to human settlements and infrastructures in many mountainous areas worldwide. Recent large-scale landslide events, such as the August 6th, 2010 Mount Meager rock slide-debris flow in Canada (Guthrie et al. 2012), the July 10th, 2013 Wulipo landslide in China (Chen and Cui 2017), and the March 22nd, 2014 Oso landslide in USA (Iverson et al. 2015), are characterized by high speed, long runout distance, and flow-like movement. Some of unstable slopes may change abruptly and move a long distance within minutes after a long period of slow deformation (Kilburn and Pasuto 2003). Different mechanisms have been proposed to explain the initiation and high mobility of the fast moving flow-like landslides, such as fluidization with entrapped air (Kent 1966), air cushion effect (Shreve 1968), pore-water pressure increasing via self-undrained loading (Sassa 1988), thermo-poro-elastic hypothesis (Goren and Aharonov 2007), velocity-weakening friction (Lucas et al. 2014), and liquefaction of water-saturated sediment at base (Iverson et al. 2015). Zhang and Yin (2013) summarized mobility controlling factors and transport mechanisms of 43 rock avalanches in China and proposed that huge kinetic energy, excessive pore-water pressure, and elastic energy released by rock fragmentation are the main causes of the long run-out rock avalanches.

A large-scale landslide happened at Xinmo village of Mao County, Sichuan Province, China at 05:39 local time on June 24, 2017 (21:39 UTC, June 23rd), causing 83 fatalities. The landslide is a rapid-moving flow-like rockslide with strong rock fragmentation and basal entrainment and can be classified as rockfall-debris avalanche, according to the most common landslide classification worldwide accepted (Cruden and Varnes 1996; Hungr et al. 2014). After the event, some research papers dealing with different aspects of the landslide have been published (Ouyang et al. 2017; Su et al. 2017; Fan et al., 2017a, b; Wang et al. 2017). They argued that the landslide was triggered by long-duration low-intensity rainfalls and took place along the major discontinuities consisting of cracks and fissures which were ascribed to a historic earthquake in 1933 with the epicenter at Diexi, 8.7 km from the village.

In order to further understand the occurrence, a field expedition was carried out in November 2017 on the mountain top at an elevation of 3430 m, where the rock slide originated, which revealed some new evidences that are inconsistent with the previous researches and reports. Besides the data provided by Su et al. (2017) and Fan et al. (2017a), more UAV and satellite images have been collected to study in-depth the cracks' characteristics and their role in the triggering mechanism. Analysis and interpretation of multi-temporal remote-sensing images as well as mechanical calculations and finite element simulations allowed a more convincing explanation of the failure mechanism.

The Xinmo landslide on June 24, 2017

Regional settings

The Xinmo landslide is located in Songping Valley, a left tributary of Minjiang River, belonging to a transition zone from the Tibet Plateau to the Western Sichuan Plain (Fig. 1). It is characterized by a temperate monsoon climate on the eastern margin of Tibetan Plateau with an average annual temperature of 11.2 °C. The average annual rainfall is 556.9 mm, approximately 90% of which is concentrated between April and October. The maximal monthly and daily rainfalls are 168.1 mm and 75.2 mm, respectively. Due to high relief, the climate shows strong local effect and significant variations with respect to elevation, which results in a broad variety of erosional landforms and landscapes (Su et al. 2017).

Geologically, the area is controlled by Jiaochang arc structure, Minjiang Fault, and Minshan Block (Fig. 1a). The main outcropping rock formations are the Triassic Zagunao Group that is composed by metamorphic sandstone interbedded with slate and partial limestone and phyllite. This complex tectonic structure-induced intensive earthquakes such as the 1933 Ms 7.5 Diexi earthquake occurred along the Songping Fault (the epicenter distance to the Xinmo village was about 8.7 km, and the seismic local intensity was X degree), the 1976 Ms 7.2 Songpan-Pingwu along the Huya Fault (the epicenter distance 67 km, and the seismic local intensity VI degree), and the 2008 Ms 8.0 Wenchuan earthquake along the Longmen Mountain Faults (the epicenter distance 120 km, and the seismic local intensity VIII degree) (Wang et al. 2017). The concealed Songping Fault has strongly conditioned the development of geological hazards along the valley. However, its location is not univocally indicated in the previous studies. For example, this structure goes through the foot of the
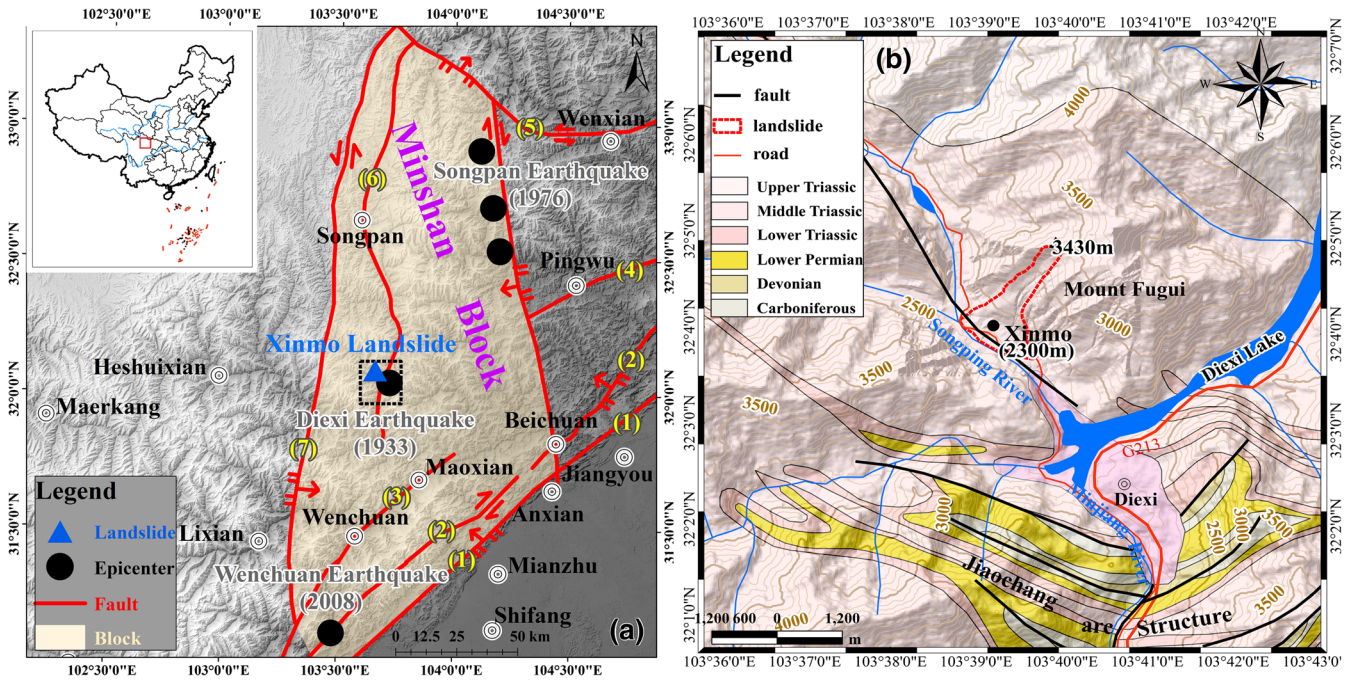
Fig. 1 The tectonic setting (**a**) and location (**b**) maps of the study area. (1) Guanxian-Anxian fault, (2) Yingxiu-Beichuan fault, (3) Maowen fault, (4) Pingwu-Qingchuan fault, (5) Tazang-Wenxian fault, (6) Minjiang fault, (7) Mounigou fault

landslide along the Songping River in Wang et al. (2017) and Su et al. (2017) while it intersects the middle part of the Xinmo landslide in Fan et al. (2017b). In this paper, the fault's location illustrated in the former two references is adopted since Wang et al. (2017) provided a convincing proof of the fault crossing the foot with the help of high-density resistivity profiles detected by AMT (audio-frequency magnetotelluric) method. More details on the geological settings of this area can be found in Su et al. (2017), Fan et al. (2017a), and Wang et al. (2017).

The investigated area is a typical alpine valley where more than 60% of hillslopes are steeper than 30°. Massive rockfall accumulations and Quaternary deposits (including fluvial deposits, eluvial deposits, and loess) distribute along the foot gentle slopes at the both sides of Songping River (Su et al. 2017). The 1933 Diexi earthquake induced many large-scale landslides which blocked Songping and Minjiang rivers, causing nine dammed lakes in Songping and other three lakes in Minjiang (e.g., Diexi Lake in Fig. 1b) (Chai et al. 1995; Xu and Wang 2005). Su et al. (2017)
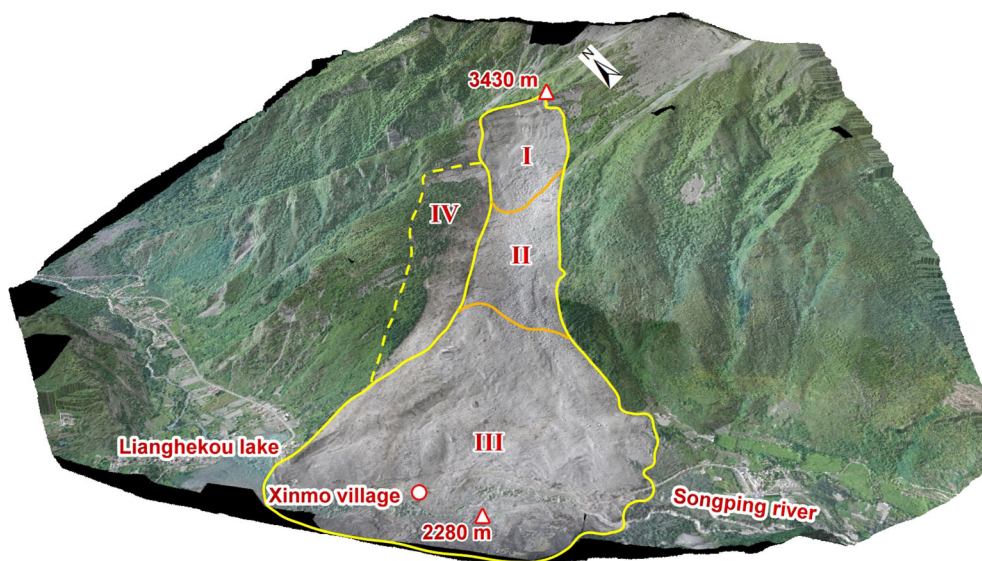

Fig. 2 3D view of the "June 24th" Xinmo landslide (I. Source zone, II. Transportation zone, III. Accumulation zone, IV. Destabilized zone)
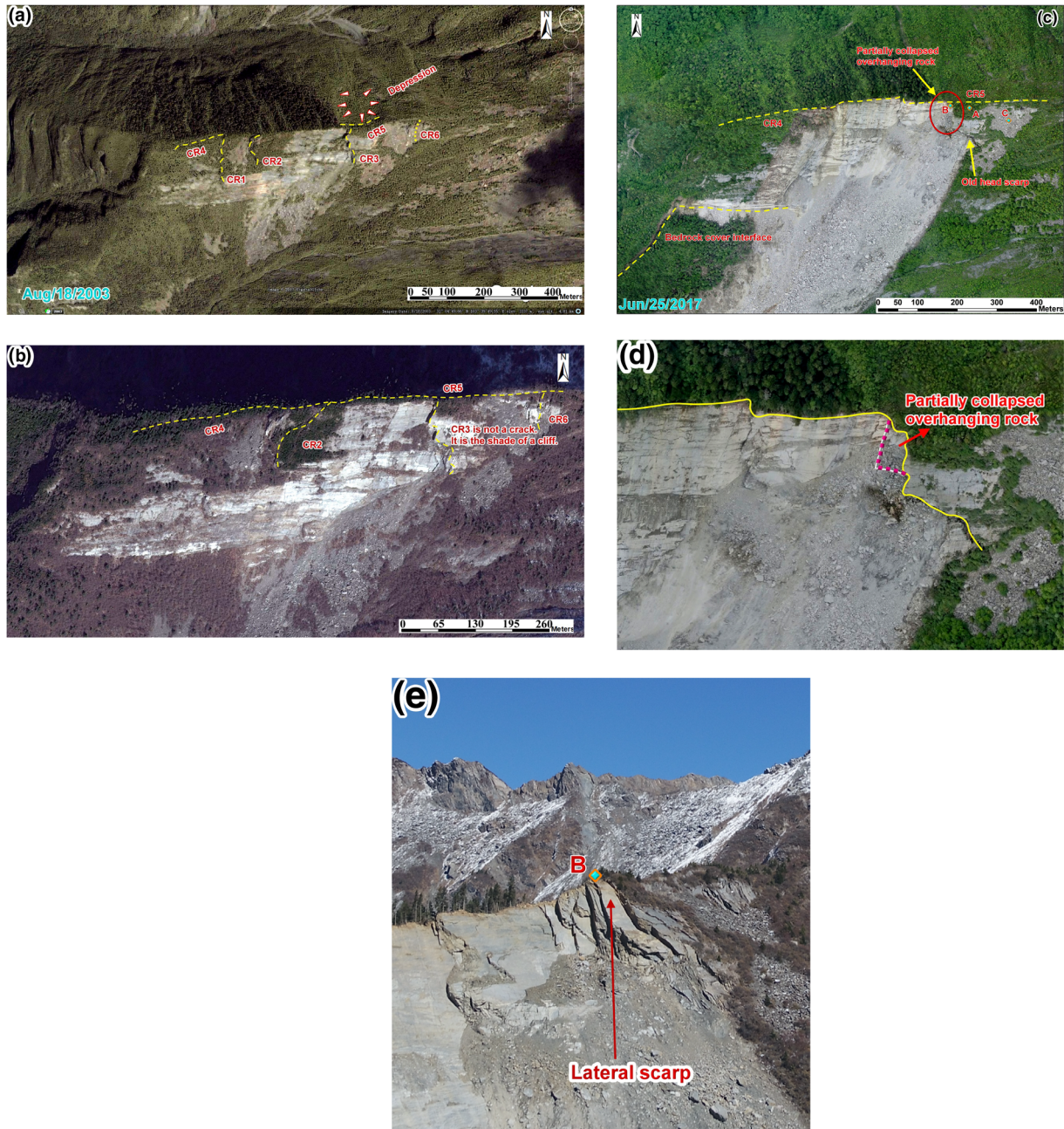
Fig. 3 Cracks in the source area before and after the June 24th event (**a** Landsat satellite image with 30 m resolution on August 18, 2003 taken from Google Earth; **b** NASA satellite image with 2.5 m resolution taken from Zoom Earth of which date is between 2009 and 2015; **c** UAV image with 0.1 m resolution on June 25th, 2017 provided by Sichuan Bureau of Surveying, Mapping and Geoinformation. Point A, B, and C correspond to the photo sites of Figs. 4a, b, and 6c; **d** enlarged partial image of **c**, the dashed purple line indicates the fallen rock; **e** UAV photo of CR3 taken on Nov. 27th, 2017, Point B is the same as that in **c**, lateral scarp is that in Fig. 4b but viewed from downslope)

located some of the old landslides caused by the 1933 earthquake in Songping river, among which is the old Xinmo landslide caused the Lianghekou lake (Fig. 2). Fan et al. (2017b) mapped the extent of the old landslide deposits.

Characteristics of the landslide

The landslide initiated at an elevation of 3430 m a.s.l on the ridge of Mount Fugui (Fig. 2). The Xinmo village at an elevation of 2300 m, 60 m higher than Songping River was completely

devastated by the June 24th event (103 destroyed buildings, 3 injured persons, and 83 persons died or missing). A volume of about 3.0 million m³ of metamorphic sandstone suddenly detached from the upper scarp, strongly eroded the channel and flanks, and entrained, during its motion, an additional volume of about 10.0 million m³ of the 1933 deposit. The moving mass blocked the Songping River and created a 1.2-km-long dam. A relative difference in elevation of 1130 m provided huge kinematic energy for the sliding body that was collided and fragmented. The
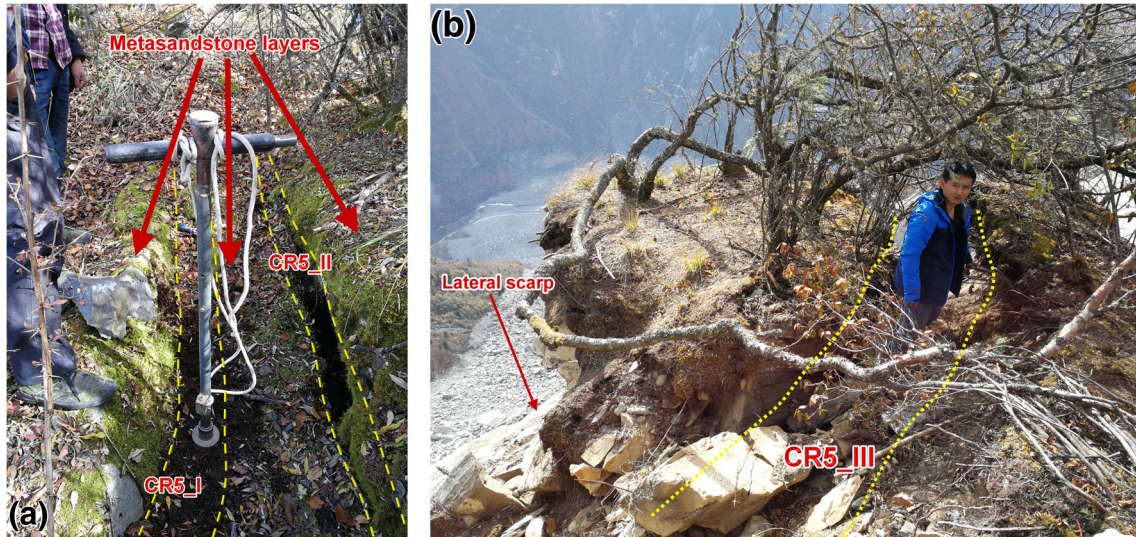
Fig. 4 Cracks on the mountain ridge (**a** two rock cracks at Point A in Fig. 3c, the lens towards east, CR5_I is about 3 m long and 15 cm wide on the Earth's surface. CR5_II is 5 m long and 10 cm wide; **b** one rock crack at Point B in Fig. 3c, the lens towards west, CR5_III is 2 m long and 1 m wide. The cliff is located behind the man)

maximum velocity of the landslide reached up to 55 m/s as shown by numerical simulations (Ouyang et al. 2017).

The whole area involved in the instability process can be roughly divided into four different zones: source zone (area = 0.15 km²), transportation zone (area = 0.29 km²), accumulation zone (area = 1.01 km²), and destabilized (or potential unstable) zone (area = 0.17 km²) (Fig. 2). The source zone was affected by a dense network of cracks which released a relevant volume of rock prone to fail. The main part of the initial moving mass came from this zone, and some rock deposits located at its base. The transportation zone is a 270-m-wide shallow channel with the average slope gradient of 55.8%. The detached rock mass accelerated in the

channel and plowed sediment on the channel bed. The erosion depth in the transportation zone was calculated by comparing pre- and post-event high-resolution digital elevation model data and is up to 38.0 m. The accumulation zone is the largest and gentlest one. The average and maximum accumulation heights are 8 m and 32 m, respectively, and the total volume has been estimated (with the above-mentioned method) as about 8.0 million m³ (Fan et al., 2017a). The destabilized zone affects the western side of the transportation zone and represents a bedrock slab mantled by slope colluvium. The Quaternary deposits became unstable and slid towards the channel due to the deep erosion caused by the high speed mass movement. This area has been completely destabilized

Soil profile	Depth (cm)	Stratum	Soil horizons	Symbol	Description
	0–30		topsoil	S₁	Black topsoil, with dead leaves and leaves of organic residues, plant roots are developed, and its thickness is less than 30 cm.
	30–40		leached horizon	S₂	Gray-black, silty clay, breccia and gravel. With relatively strong weathering, this layer is rich in organic matter. The soil seems very loose owing to development of granular structure.
	40–90		loess	S₃	Bright-yellow brown, silty clay. Homogeneous texture, moderate weathering and loose soil. With medium dense, this layer developed nucleolus granular structure.
	90–100		mixed horizon	S₄	Gray-black sandy clay, fine sand, with breccia and gravel. The mixed horizon is very loose. Weak weathering, nucleating granular structure, the layer is in contact with the bedrock.

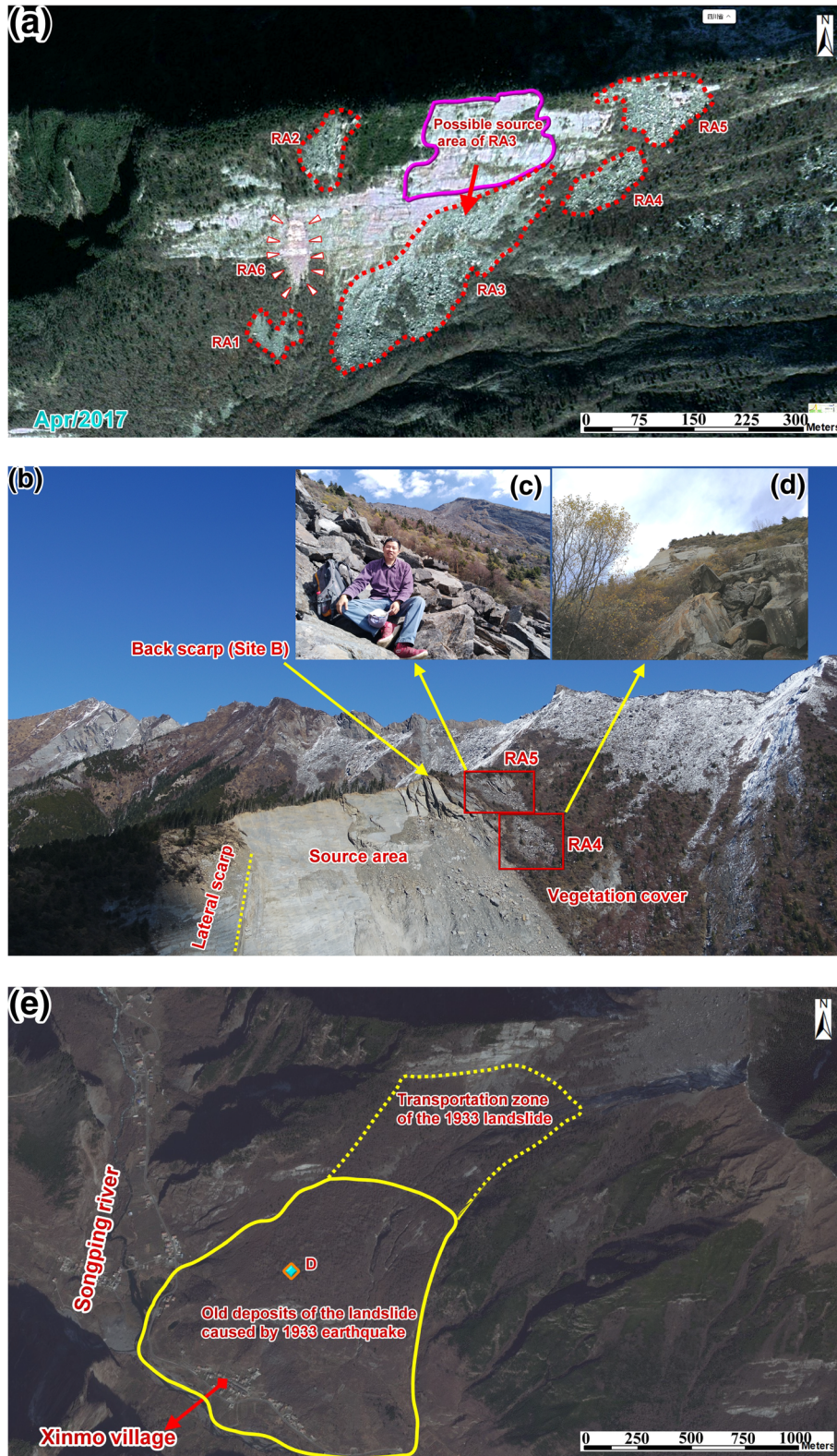**Fig. 5** Soil deposition profile at Point B on the mountain ridge

Fig. 6 Previous rock avalanche deposits and the source area of the June 24th event on the ridge (**a** Gaofen-2 satellite image with 2.5 m resolution on April 8th, 2017 taken from Tianditu; **b** UAV image taken on Nov. 27th, 2017; **c** field photo of RA5 taken on Nov. 13th, 2017; **d** field photo of RA5 taken on Nov. 13th, 2017; **e** NASA satellite image taken from Zoom Earth, Point D is the location of the huge rock block in Fig. 8, solid outline is the area of the old landslide deposits from Fan et al. (2017a), dash outline is the transportation zone of the old landslide)

Table 1 Basic information of the six rockfall deposits derived from Gaofen-2 image

No.	Deposition area (m²)	Time occurrence	Images with rockfall's mark
RA1	5080	Before Aug. 18th, 2003	Landsat, NASA and Gaofen-2 satellites
RA2	5458	Before Aug. 18th, 2003	Landsat, NASA and Gaofen-2 satellites
RA3	50,109	Before Aug. 18th, 2003	Landsat, NASA and Gaofen-2 satellites
RA4	5332	Before Aug. 18th, 2003	Landsat, NASA and Gaofen-2 satellites
RA5	7228	Before Aug. 18th, 2003	Landsat, NASA and Gaofen-2 satellites
RA6	3390	Between 2016 and 2017	Gaofen-2

by the June 24th event, and from June 29th to July 4th, the averaged cumulative displacement of six monitored benchmarks in the eastern and rear parts of the zone reached the value of 93 mm (Fan et al., 2017b).

Structural analysis of the source area

Recent scientific papers describe the existence of cracks in the source area before the event (Su et al. 2017; Fan et al., 2017b; Wang et al. 2017). The top cracks on the ridge and the lateral radial cracks on the both sides of the source area are likely related to previous earthquakes, tectonic lineaments, namely Jiaochang arc belt and lithological characteristics of the outcropping sequence (e.g., slate intercalations) (Wang et al. 2017). They argued that the crack network affecting the dip slope was caused by the 1933 Diexi earthquakes and developed by subsequent strong earthquakes. The field investigations confirmed the existence of such cracks except the one on the eastern flank.

Remote-sensing interpretation of the cracks

In order to study the development of crack network, multi-temporal remote sensing and UAV images have been collected and compared (Fig. 3). Two groups of cracks have been detected in the source area: main cracks along the top of the ridge and lateral cracks on the both sides of the area. The first group includes cracks 4 and 5 (Fig. 3a, b) recognized also by Su et al. (2017) and Fan et al. (2017a). However, they were considered as a single connected fracture with a length of about 750 m developed along the bedrock striking direction of N 80° W (Fig. 3b).

The second group is composed by CR1, CR2, and CR6 that are lateral cracks on the east and west flanks, intersecting with the main cracks at an acute angle (Fig. 3a, b). These cracks are shorter than the main ones and formed the lateral scarps of the landslide. This group is believed to concur with the 1933 earthquake because its main direction is parallel to the seismogenic fault (i.e., the Songping Fault) of the earthquake (Fig. 1). Another crack, the so-called CR3, was also identified by some researchers (Su et al. 2017; Fan et al., 2017a) (Fig. 3a, b), but it is not a real crack, just the shade of the overhanging rock which is a lateral scarp of a past detachment. Therefore, the so-called crack 3 is not the east flank of the June 24th landslide (Fig. 3b, c) but simply the head scarp of an old rockfall. Comparing the UAV image after the June 24th event with the Zoom Earth image and high-resolution UAV image (Fig. 3c, d), it is clear that part of the overhanging rock collapsed in the event. The photo taken by UAV on Nov. 27th, 2017 shows clearly the remnant of the hanging rocks (Fig. 3e). In addition, a depression on the opposite side of the ridge indicates the existence of more cracks, not clearly interpreted due to dense vegetation cover.

Characteristics of the main cracks on the top of the mountain ridge

The main cracks mentioned above are actually composed by several minor parallel deep tensile cracks with the same orientation of the bedding planes between the intercalated slate and metasandstone. Three fractures (CR5_I, CR5_II, and CR5_III, in Fig. 4) surveyed at the sites A and B (cfr. Fig. 3c) are part of the CR5, and their orientation is in accordance with the rock stratum. These fractures extend from the upper part of the ridge and end at the site B where a cliff formed because part of the ridge's top fell down in the June 24th event (Fig. 3e). The rock layer between CR5_I and CR5_II is about 40 cm thick, and the distance from the cracks to the edge of the ridge is 5 m. The fractures are partially filled with leaves and humus soil. The ^{137}Cs analysis of the filling material shows that the formation of the two cracks was not later than 1963.
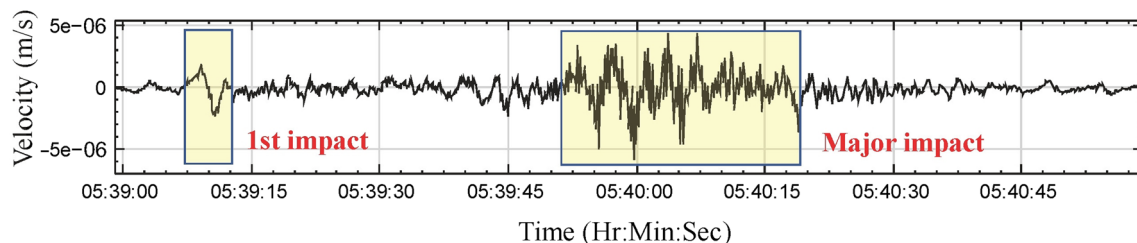

Fig. 7 Broadband seismograms of the June 24th landslide recorded at the Maoxian seismic station (vertical direction, courtesy from Prof. ZHAO Yong, China Earthquake Networks Center)
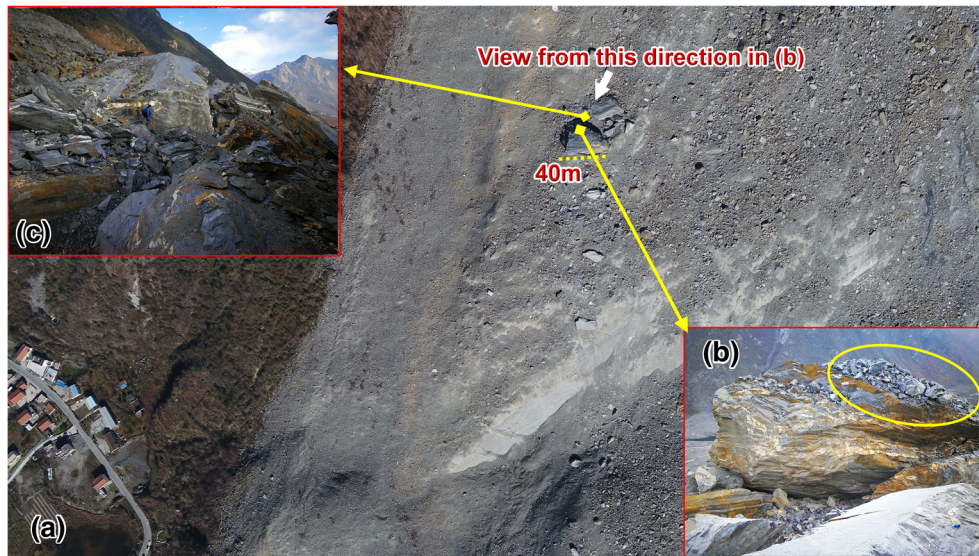
Fig. 8 The broken huge rock block docked at Point D (Fig. 7) in the accumulation area (**a** UAV photo taken on Nov. 27, 2017; **b** lower part of the broken rock block, the yellow circle is debris deposited on the block's surface, view along slide direction; **c** upper part of the broken rock block, the man's height is about 1.7 m)

CR5_III is located at the top of the June 24th landslide's back scarp (Fig. 4b). The broken tree roots and separated vegetation and covered soil show that the rock on the right moved downslope of about 1 m. CR5_III was widened 1 m due to the shifted rock. The rock covered by trees and 40-cm-thick soil on the right hand of the man in Fig. 4b are the remnants of the surface rock layer most of which fell down in the June 24th event. In Fig. 4b, on the left hand of the man, there is a soil layer 1.0 m thick and the top soil layers on the both sides of CR5_III are similar. Four layers including mixed horizon, loess, leached horizon, and topsoil can be recognized on the soil section (Fig. 5). It appears likely from the covered soil and vegetation that the main cracks may be very old and formed by long-term weathering, tectonic movements, and ancient earthquakes well before 1933.

Evidences of small-scale rockfalls in the source zone

Previous rockfall events
The Gaofen-2 satellite image indicates at least six rock deposits of different sizes in the source area (Fig. 6a), which obviously came from recent rockfalls and favored by the dense crack network. The largest deposit is RA3 and the smallest is RA6 (Table 1). RA4 and RA5 are located in the upper part of the source area near the ridge, and thus, the failed mass should be basically accumulated very close to the detachment area (Fig. 6b). RA6 is the most recent one because no evidences are visible in the Google Earth and Zoom Earth images taken in 2016. RA3 also originated from the same region of the June 24th event and CR3 can be considered the back scarp of the originating rockfall. It is observed that RA1 and RA5 deposits are partially covered by vegetation most likely grown up since a large-scale landslide triggered by the 1933 earthquake (Xu and Wang 2005; Wang et al. 2008) (Fig. 6c, d). According to Fan et al. (2017b), the old landslide deposits caused by the 1933 earthquake covered a larger area than the June 24th event. That means the vegetation before the earthquake was destroyed completely by the old landslide, and the present vegetation was recovered after that (Fig. 6e). These evidences are very important in pointing out the proneness of the source zone in rockfalling, especially after the Diexi earthquake and in highlighting the role of an initial rockfall in triggering the June 24th event which completely entrained the 1933 landslide deposit thus greatly increased its volume (Su et al. 2017; Fan et al., 2017a).

Precursory small-scale rock fall in the June 24th event
In many cases, the temporal and spatial evolution of large-scale landslides can be inferred from their seismic records (Caloi 1966; Schneider et al. 2010; Guthrie et al. 2012; Allstadt 2013; Moretti et al. 2015). One of the first attempt to infer the dynamic evolution of a landslide and related effects (in that case the water wave propagation) from seismic data is illustrated in Caloi (1966) which described the case of Vajont landslide and the investigations carried out since the beginning of the reservoir filling up. As for the specific case of precursory smaller events triggering complex landslide (cfr. Cruden and Varnes 1996), Guthrie et al. (2012) and Allstadt (2013) detected similar precursory of nearly vertical collapses at the beginning of the August 2010 Mount Meager landslide from recorded seismograms. The Xinmo landslide caused an earthquake of Ms 2.2 which was recorded by 33 seismic stations. The data recorded at Maoxian Seismic Station 48 km south to the Xinmo village indicates that something happened in the very early phase of the June 24th event (Fig. 7). The first pulse at 05:39:07 (local time) is therefore interpreted as a near-vertical collapse from the upper scarp that impacted the bedrock in the source area and triggered a continuous rock blocks rolling until the main larger rock failure, producing the higher and longer amplitude wave (from 05:39:52 to 05:40:20), took place (Zhao 2017; Bai et al. 2018; Zhao 2018). Soon after, the high speed rock mass impacted on the channel and lower slope entraining old landslide deposits and turning into a rock avalanche, before rushing to the opposite river bank climbing up about 100 m.
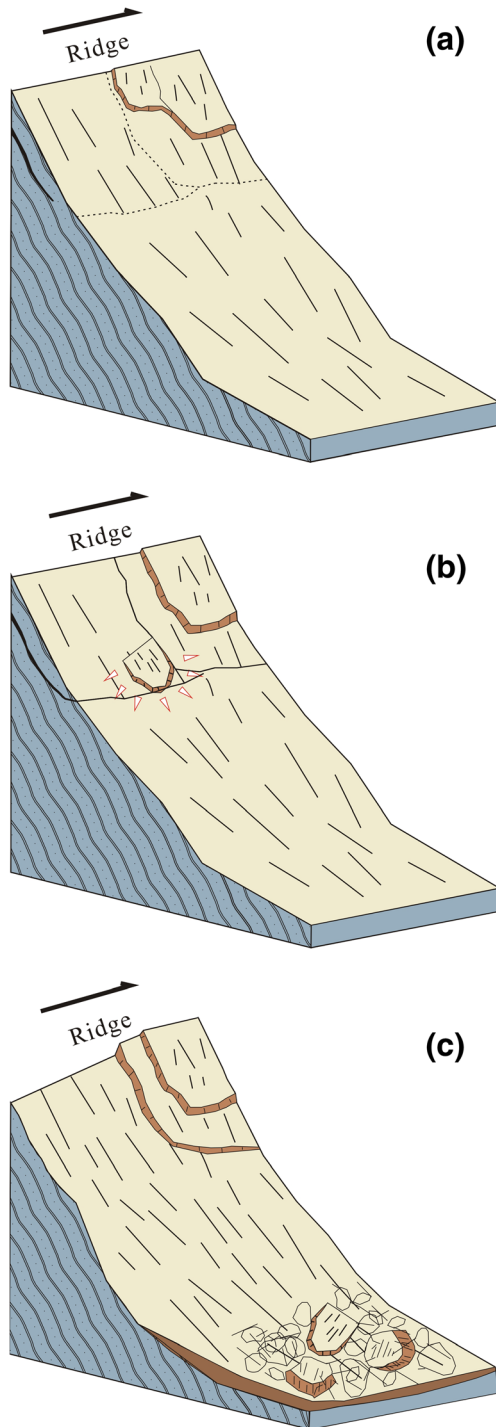
Fig. 9 Schematic illustration of the proposed triggering mechanism of the June 24th event (**a** the original rock mass, although affected by a crack network, was locked by persistent rock bridges at bottom and laterally; **b** the hanging rock at the CR3 nearly vertically collapsed and impacted the connection location, the cracks propagated rapidly; **c** the fast-moving main body fragmented and deposited)

Moreover, the finding of a huge rock block in the lower accumulation area also confirms the initial small rockfall (Fig. 8). The rock block stopped at the elevation of 2580 m and broke up into three large parts. The largest part's dimension is about 40 m long, 35 m wide, and 10 m high, and its lithological composition of metamorphic sandstone indicates that it has been detached from the upper scarp. The rock block is partially covered by fresh debris plentiful accumulated at the back (mountain side) and on the top (yellow circle in the Fig. 8b). This implies that it fell before the rock avalanche completely developed. It is likely that the following rock avalanche passed by it depositing some material behind and on the top of it.

Discussions

It is no doubt that the June 24th Xinmo landslide was resulted from a combination of past strong earthquakes, tectonic movement, long-term rainfall and infiltration, and weathering processes. Previous studies concluded that the direct triggering factor was the long-duration rainfall more than 1 month before the event (Su et al. 2017; Fan et al., 2017b; Wang et al. 2017). However, the maximum daily rainfall from May 1st to June 24th was recorded up to 27 mm/24 h by three weather stations. The cumulative rainfall was about 215 mm during the whole period. Rainfall events with such intensities are not rare in this region and it is hard to explain how such normal rainfall can trigger such a large-scale rockfall-debris avalanche. Indeed for the small initial rockfall, the rainfall and the frost-thaw cycles may be really its triggering mechanism after long-term gravity drag and earthquakes. Assuming a progressive decrease in rock strength due to its aging and stress caused by external causes (e.g., earthquakes, weathering, intense rainfalls) "the slope failed when it was ripe to for failure, at a time when the factor of safety assumed one of its periodic minimum values" (Terzaghi 1950).

Based on the new understandings about cracks, rockfall deposits, and small-scale precursory events in the source zone, a different triggering mechanism for the Xinmo landslide is proposed (Fig. 9). The whole event is conjectured to be triggered by an initial small (with respect to the magnitude of the landslide occurred) rockfall event. At first, the original rock mass, although affected by a crack network, was locked by persistent rock bridges at the bottom and lateral sides of the source zone; old cracks did not develop so deeply, and the entire slide surface was not yet formed (Fig. 9a). Secondly, the hanging rock at the CR3 nearly vertically collapsed and impacted the lower part of the source area thus allowing a rapid propagation of the existing cracks until the formation of a continuous failure surface (Fig. 9b). Thirdly, the failed main rock body ran at very high speed and impacted with bumps and channel walls. The fast-moving rock fragments entrained old landslide deposits turning into a rock avalanche before they deposited finally at the foot of the mountain (Fig. 9c).

The survey data are used to calculate the pore-water pressure and the rockfall impact force exerted on the locked segment. It is assumed that the gaps were saturated, and the water pressure completely loaded on the segment. Then, the total force due to pore water can be calculated by integrating the water pressure over the slide's surface (Table 2). The fallen rock was about 60 m long, 40 m wide, and 10 m high measured with the UAV image on June 25th, 2017 and the field work. If it is a kind of elastic impact between the initial fallen block and the base old source zone which can be described by Hertz contact theory, and the mechanical energy conservation is obeyed, the maximum impact force of the

Table 2 Comparison of surface force and rockfall impact force exerted on the locked segment

Surface force due to pore water pressure	Rockfall impact force
$U_{max} = PSsin\alpha = sin\alpha\int_o^H \rho ghldh$	$F_{max} = 1.944(mgh)^{0.6}E^{0.4}R^{0.2}$
U_{max}-------- the surface force caused by pore water pressure (N) P------- pore water pressure (Pa) S -------- contact area between pore water and locked rock mass (m^2) α-------- slope angle (= 47°) H-------- the total height from the top scarp to the locked segment (= 140 m) ρ -------- density of water (= 1.0×10^3 kg/m^3) g -------- gravitational acceleration (= 9.8 m/s^2) h-------- the height of each rock element to the locked segment (m) l -------- crack length (= 230 m)	F_{max}-------- the force of the locked rock mass root in the rockfall (N) ρ-------- density of rock (= 2.5×10^3 kg/m^3) m -------- mass of the falling rock (= 6.0×10^7 kg) g --------- gravitational acceleration (= 9.8 m/s^2) h --------- the falling height (= 180 m) $^*E$-------- Effective contact elastic modulus (= 5.5×10^4 MPa) R -------- Effective contact radius (= 40~60 m)
$U_{max} = 1.62 \times 10^{10}$(N)	$F_{max} = 4.83 \times 10^{12} \sim 7.25 \times 10^{12}$ (N)

$^*E$ is set to a typical value (5.5×10^4 MPa) for such metamorphic sandstone (density = 2.5×10^3 kg/m^3) according to "Engineering Geology Manual" (Chang and Zhang 2007)

rock falling from 180-m-high slope on the base rock could be 4.83×10^{12} N (or 7.25×10^{12} N) with the effective contact radius of 40 m (60 m). In addition, a popular finite element software LS-DYNA was used to simulate the impact process of the fallen rock. The maximum impact force F_{max} is equal to 7.351×10^{11} N if the rock material is described by linear elastic constitutive model, or to 4.584×10^{11} N if described by Holmquist-Johnson-Cook constitutive model. In these cases, the impact force is one or two orders of magnitude larger than the total pore water pressure, and thus, the large-scale event was more likely triggered by the precursory small rockfall and not by the long-duration rainfall. Similar triggering mechanism was also proposed in the 2010 Mount Meager landslide (Guthrie et al. 2012).

Accordingly, it is impossible to predict the scale of such landslides even if the timing and location can be predicted or monitored very accurately. As mentioned above, several small-scale rockfalls happened in the source area in the past, some of them even larger than the precursory one recorded on the June 24th event, but they did not produce a domino effect. According to the self-organized criticality theory, sand-pile dynamical systems with extended spatial degrees of freedom can evolve into a self-organized critical state at which a further small perturbation can trigger an avalanche on any length scales (Bak et al. 1987; Bak et al. 1988). But one can never know which grain of sand will trigger a large sand avalanche. Similarly, if the Xinmo mountain slope is at a critical point, rock avalanches of any size could happen. This means the precursory events may be or may not be useful to predict this type of landslides, although it is a possible triggering factor. Therefore, from a prevention point of view, it is more important to recognize such slope systems at self-organized critical points, providing a comprehensive and reliable inventory than to monitor precursory signals trying to predict the slope failure's timing.

Conclusions

The Xinmo landslide of 24 June 2017 has been considered as related to the 1933 Diexi earthquake and directly triggered by long-duration rainfalls. This study proposes new understandings of the landslide evolution based on further remote-sensing images and field investigations. It has been found that two different groups of cracks in the source area, and at least six rock avalanches happened before the June 24th event highlighting the proneness of the source zone to rockfalls. Furthermore, the seismograms and on-spot huge rock block mapped in the landslide accumulation indicate that a nearly vertical rock collapse happened initially at the top of the slope. The small-scale rockfall is probably related to an overhanging rock slab at the scarp's summit that was previously wrongly interpreted as a crack. These findings suggest that the landslide event was caused by the impact of the initial rockfall on the locked segment. This new explanation also highlights the limitation in predicting such kinds of landslides.

References

Allstadt K (2013) Extracting source characteristics and dynamics of the august 2010 mount meager landslide from broadband seismograms. J Geophys Res Earth Surf 118:1472–1490. https://doi.org/10.1002/jgrf.20110

Bai XQ, Jian JH, He SM, Liu W (2018) Dynamic process of the massive Xinmo landslide, Sichuan (China), from joint seismic signal and morphodynamic analysis. Bull Eng Geol Environ https://doi.org/10.1007/s10064-018-1360-0

Bak P, Tang C, Wiesenfeld K (1987) Self-organized criticality: an explanation of 1/f noise. Phys Rev Lett 59:381–384

Bak P, Tang C, Wiesenfeld K (1988) Self-organized criticality. Phys Rev A 38:364–374. https://doi.org/10.1103/PhysRevA.38.364

Caloi P (1966) L'evento del Vajont nei suoi aspetti geodinamici. Ann Geofis 17(4):1–74 (in Italian)

Chai HJ, Liu HC, Zhang ZY (1995) Landslide dams induced by Diexi earthquake in 1933 and its environmental effect. J Geol Hazards Environ Preserv 6(1):7–17 (in Chinese)

Chang SB, Zhang SM (2007) Engineering geology manual, 4th edn. China Architecture & Building Press, Beijing, p 170 ISBN:9787112088287 (in Chinese)

Chen XZ, Cui YF (2017) The formation of the Wulipo landslide and the resulting debris flow in Dujiangyan City, China. J Mt Sci 14:1100–1112. https://doi.org/10.1007/s11696-017-4392-1

Cruden DM, Varnes DJ (1996) Landslides investigation and mitigation, transportation research board. In: AK turner, RL Schuster (eds) landslide types and process. National Research Council, National Academy Press, Special Report 247:36–75

Fan JR, Zhang XY, Su FH, Ge FH, Tarolli P, Yang ZY, Zeng C, Zeng Z (2017a) Geometrical feature analysis and disaster assessment of the Xinmo landslide based on remote sensing data. J Mt Sci 14:1677–1688. https://doi.org/10.1007/s11629-017-4633-3

Fan X, Xu Q, Scaringi G, Dai L, Li W, Dong X, Zhu X, Pei X, Dai K (2017b) Failure mechanism and kinematics of the deadly June 24th 2017 Xinmo landslide, Maoxian, Sichuan, China. Landslides 14:2129–2146. https://doi.org/10.1007/s10346-017-0907-7

Goren L, Aharonov E (2007) Long runout landslides: the role of frictional heating and hydraulic diffusivity. Geophys Res Lett 34:L07301. https://doi.org/10.1029/2006GL028895

Guthrie RH, Friele P, Allstadt K, Roberts N, Evans SG, Delaney KB, Roche D, Clague JJ, Jakob M (2012) The 6 august 2010 mount meager rock slide-debris flow, Coast Mountains, British Columbia: characteristics, dynamics, and implications for hazard and risk assessment. Nat Hazards Earth Syst Sci 12:1277–1294. https://doi.org/10.5194/nhess-12-1277-2012

Hungr O, Leroueil S, Picarelli L (2014) The Varnes classification of landslide types, an update. Landslides 11(2):167–194. https://doi.org/10.1007/s10346-013-0436-y

Iverson RM, George DL, Allstadt K, Reid ME, Collins BD, Vallance JW, Schilling SP, Godt JW, Cannon CM, Magirl CS, Baum RL, Coe JA, Schulz WH, Bower JB (2015) Landslide mobility and hazards: implications of the 2014 Oso disaster. Earth Planet Sci Lett 412:197–208. https://doi.org/10.1016/j.epsl.2014.12.020

Kent PE (1966) The transport mechanism in catastrophic rock falls. J Geol 74:79–83. https://doi.org/10.1086/627142

Kilburn CRJ, Pasuto A (2003) Major risk from rapid, large-volume landslides in Europe (EU project RUNOUT). Geomorphology 54(1–2):3–9

Lucas A, Mangeney A, Ampuero JP (2014) Frictional velocity-weakening in landslides on earth and on other planetary bodies. Nat Commun 5(3417). https://doi.org/10.1038/ncomms4417

Moretti L, Allstadt K, Mangeney A, Capdeville Y, Stutzmann E, Bouchut F (2015) Numerical modeling of the mount meager landslide constrained by its force history derived from seismic data. J Geophys Res Solid Earth 120:2579–2599. https://doi.org/10.1002/2014JB011426

Ouyang CJ, Zhao W, He SM, Wang DP, Zhou S, An HC, Wang ZW, Cheng DX (2017) Numerical modelingand dynamic analysis of the 2017 Xinmo landslide in Maoxian County, China. J Mt Sci 14:1701–1711. https://doi.org/10.1007/s11629-017-4613-7

Sassa K (1988) Geotechnical model for the motion of landslides. In: Bonnard C (ed) Landslides, proc 5th ISL, Lausanne. Balkema, Rotterdam, pp 37–55

Schneider D, Bartelt P, Caplan-Auerbach J, Christen M, Huggel C, McArdell BW (2010) Insights into rock-ice avalanche dynamics by combined analysis of seismic recordings and a numerical avalanche model. J Geophys Res 115:F04026. https://doi.org/10.1029/2010JF001734

Shreve RL (1968) The Blackhawk landslide. Geol Soc Am Spec Pap 108:47

Su L, Hu K, Zhang W, Wang J, Lei Y, Zhang C, Cui P, Pasuto A, Zheng Q (2017) Characteristics and triggering mechanism of Xinmo landslide on 24 June 2017 in Sichuan, China. J Mt Sci 14:1689–1700. https://doi.org/10.1007/s11629-017-4609-3

Terzaghi K (1950) Mechanisms of landslides. In: Application of Geology to Engineering Practice, Geol Soc of America, Berkeley 83–125. https://doi.org/10.1130/Berkey.1950

Wang LS, Yang LZ, Li TB, Xu XN, Wang XQ, Cui J (2008) Diexi earthquake-induced landslide, Min River, Sichuan Province (1933). In: R Huang, Q Xu (eds) catastrophic landslides in China 57–93 science press Beijing ISBN: 9787030223500 (in Chinese)

Wang Y, Zhao B, Li J (2017) Mechanism of the catastrophic June 2017 landslide at Xinmo Village, Songping River, Sichuan Province, China. Landslides 15:333–345.https://doi.org/10.1007/s10346-017-0927-3

Xu XN, Wang LS (2005) On the mechanism of slope deformation-failures and their distribution characteristics in a high earthquake-intensity area. J Eng Geol 13(1):68–75 (in Chinese)

Zhang M, Yin YP (2013) Dynamics, mobility-controlling factors and transport mechanisms of rapid long-runout rock avalanches in China. Eng Geol 167:37–58. https://doi.org/10.1016/j.enggeo.2013.10.010

Zhao J (2018, 2018) Seismic signals analysis of the June 2017 Maoxian landslide. Japan Geoscience Union Meeting:HDS07–HDP09

Zhao Y (2017) Process analysis of Maoxian landslide on June 24th, 2017. http://t.girtu.com/post/show/5955aafacb70f290780c883b. (in Chinese)

K. Hu · C. Wu · J. Tang · Y. Li · S. Yan
Key Laboratory of Mountain Hazards and Earth Surface Processes,
Chinese Academy of Sciences,
Chengdu, 610041, China

K. Hu (✉) · C. Wu · J. Tang · Y. Li · S. Yan
Institute of Mountain Hazards and Environment,
Chinese Academy of Sciences,
Chengdu, 610041, China
Email: khhu@imde.ac.cn

C. Wu · Y. Li · S. Yan
University of Chinese Academy of Sciences,
Beijing, 100049, China

A. Pasuto
National Research Council of Italy-Research Institute for Geo-Hydrological Protection,
Padova, Italy